

Minimum conductivity and charge inhomogeneity in Bi_2Se_3 in the topological regime

Dohun Kim*, Sungjae Cho*, Nicholas P. Butch, Paul Syers, Kevin Kirshenbaum, Johnpierre Paglione, and Michael S. Fuhrer⁺

Center for Nanophysics and Advanced Materials, Department of Physics, University of Maryland, College Park, MD 20742-4111, USA

The newly-discovered three-dimensional strong topological insulators (STIs) exhibit topologically-protected Dirac surface states^{1,2}. While the STI surface state has been studied spectroscopically by e.g. photoemission³⁻⁵ and scanned probes⁶⁻⁹, transport experiments¹⁰⁻¹⁶ have failed to demonstrate the most fundamental signature of the STI: ambipolar metallic electronic transport in the topological surface state of an insulating bulk. Here we show that the surfaces of thin (<10 nm), low-doped Bi_2Se_3 (<10¹⁷/cm³) crystals are strongly electrostatically coupled, and a gate electrode can be used to completely remove bulk charge carriers and bring both surfaces through the Dirac point nearly simultaneously. We observe clear ambipolar electronic conduction with well-defined *p*- and *n*- regions, as well as a charge-inhomogeneous minimum conductivity region similar to that observed in graphene¹⁷⁻¹⁹. An extension of the theory of charge disorder in graphene^{18,19} to Bi_2Se_3 ²⁰ explains well the minimum conductivity value (3-5 e^2/h per surface), the residual puddle carrier density (1.3 – 2.6 x 10¹² cm⁻²), the mobility at high carrier density (400 – 1,000 cm²/Vs), and the doping level at zero gate voltage (~3 x 10¹³ cm⁻²) assuming a charged impurity density of 3-13 x 10¹³ cm⁻².

*these authors contributed equally to this work.

Bi_2Se_3 as prepared is observed to be n -type due to Se vacancies. We find that mechanically exfoliated thin (thickness $t \sim 10$ nm) Bi_2Se_3 on SiO_2/Si is invariably highly n -doped with sheet charge densities $>10^{13} \text{ cm}^{-2}$, much greater than the expected considering the bulk charge density ($\sim 10^{17} \text{ cm}^{-3}$) in our low-doped starting material²¹, suggesting additional doping is induced by mechanical cleavage, reaction with ambient species^{13,22}, or substrate interaction. In order to remove this doping, we fabricated mechanically-exfoliated thin Bi_2Se_3 field-effect transistors on 300 nm SiO_2/Si back gate substrates with an additional polymer electrolyte top gate²³⁻²⁵ (polyethylene oxide/ LiClO_4 ; see Methods).

Figure 1a shows a schematic of device structure and the inset shows an optical image of representative device. Ionic gating exploits large capacitance ($\sim \mu\text{F}/\text{cm}^2$) of the electrochemical double layer at the interface between accumulated ions and sample surface²³⁻²⁵. The maximum carrier density that can be tuned by the solid polymer electrolyte is mainly limited by the onset of electrochemical reactions of the ions with the sample. To minimize such reactions, the device was rapidly cooled down to low temperature (~ 5 K) after applying the top gate voltage²⁴, and the back gate was used to further tune the carrier density (see Methods section).

Figure 1b shows the resistivity ρ and Hall carrier density $n_H = 1/R_H e$ (where R_H is the Hall coefficient, and e is the elementary charge) of device 1 (run 1) at various temperatures from 5 K to 63 K as a function of back gate voltage. $\rho(V_g)$ shows a peak at approximately $V_{g,0} = -80$ V, and n_H changes sign at a similar V_g , diverging positively (negatively) when approaching $V_{g,0} = -80$ V from above (below). The behavior is strongly reminiscent of that seen in graphene¹⁷. Likewise, we identify the linear regions of n_H vs V_g for $V_g > -60$ V and $V_g < -95$ V as uniformly n - and p -doped regimes respectively, and the region $-65 < V_g < -95$ V as an inhomogeneous

regime where electron and hole transport are both present. The temperature dependence of the resistivity is everywhere metallic, saturating at low temperature. As we argue below, this represents the first experimental demonstration of metallic, ambipolar, gapless electronic conduction of the topological surface state in Bi_2Se_3 in the absence of bulk carriers, the defining quality of a topological insulator.

We note that a previous work on singly-gated Bi_2Se_3 of similar thickness but heavily (0.5%) Ca-doped¹⁶ also showed a superficially similar resistivity peak, however significant band-bending led to very different carrier densities on either side of the device and a large temperature dependence of n_{H} and $V_{\text{g},0}$ not observed here. The authors identified the peak with the depletion of the conduction band, and the unipolar n -type Hall regime as the population of the conduction band. No unipolar p region was observed, and no quantitative measurement of the carrier-density-dependent surface state conductivity was made. Other experiments which probe only one TI surface in the presence of a conducting bulk^{10,12,16} are difficult to interpret quantitatively, and are unlikely to be able to measure e.g. the minimum conductivity or charge inhomogeneity.

The slope $dn_{\text{H}}/dV_{\text{g}}$ is used to estimate the total capacitive coupling $C_{\text{g,tot}} = 28 \text{ nF/cm}^2$ of the back gate to the Bi_2Se_3 crystal. The 300 nm SiO_2 has a capacitance of $C_{\text{g,b}} = 12 \text{ nF/cm}^2$ to the bottom surface, and the additional capacitance of $C_{\text{g,t}} = 16 \text{ nF/cm}^2$ reflects coupling through the surrounding SiO_2 and highly-polarizable (though insulating) polymer electrolyte to the top surface of the Bi_2Se_3 . The near-equivalence of $C_{\text{g,b}}$ and $C_{\text{g,t}}$ helps to ensure similar carrier densities are induced on each surface and limit band bending¹⁶. However, in thin, lightly doped Bi_2Se_3 the surfaces are also strongly electrostatically coupled which greatly enhances the tendency to equalize their surface charge densities. In the limit that the surface states are perfect metals (quantum capacitance $C_{\text{q}} \rightarrow \infty$) the back gate would couple only to the bottom surface

state. However, for a Dirac surface state with $v_F = 6.4 \times 10^5 \text{ m/s}^{2,3,5,8,9}$, $C_q = e^2 D(E_f) = 0.5 \text{ } \mu\text{F/cm}^2$ for carrier densities $n = 0.5 \times 10^{12} \text{ cm}^{-2}$. Thus C_q is less than the inter-surface electrostatic capacitance $C_{il} \approx 9 \text{ } \mu\text{F/cm}^2$ for bulk Bi_2Se_3 with relative dielectric constant $\kappa \approx 100$ [21] and $t = 10 \text{ nm}$. In the limit that $C_{il} \gg C_q$, the two surfaces are strongly coupled and their Fermi energies move together with gating. The experimental observations suggest we approach this limit. For the parameters above, we estimate that the charge density difference between top and bottom layers near the Dirac point is less than $0.3 \times 10^{12} \text{ cm}^{-2}$, much smaller than the observed region of combined electron and hole transport (see also Supplementary Information). A finite depth of the surface states will increase C_{il} . Below, we report the transport properties as a function of carrier density per surface n estimated from $n = (C_{g,\text{tot}}/2e)(V_g - V_{g,0})$ where $V_{g,0}$ is the gate voltage at which $R_H = 0$, which corresponds closely to the gate voltage of minimum conductivity.

We now examine surface electronic transport of Bi_2Se_3 in the TI regime. Figure 2 shows (a) conductivity per layer (σ), (b) the Hall carrier density per layer ($n_{H,\text{layer}} = 1/2R_H e$), and (c) field effect mobility $\mu = \sigma/ne$ vs. carrier density at $T = 5 \text{ K}$. Data are shown for device 1 for the device cooled rapidly (run 1) and with a $\sim 5 \text{ min}$ delay (run 2) after application of the electrochemical gate voltage and additional devices (device 2 and 3). Several features are notable immediately in Figure 2 and comprise the major experimental observations in this work. Upon carrier density tuning, (1) σ and n_H show clear ambipolar conduction with well-defined p - and n -regions, (2) $|n_{H,\text{layer}}|$ shows a minimum value (n^*) for p - and n -conduction, (3) σ shows a linear carrier density dependence for $n^* < n < n_{\text{bulk}}$ where $n_{\text{bulk}} \approx 5 \times 10^{12}/\text{cm}^2$ is the carrier density above which the bulk conduction band is expected to be populated, and (4) a minimum conductivity ($\sigma_{\text{min}} = 3.5 e^2/h$) is observed.

Extending the theory of charge disorder in graphene^{18,19}, a recent theoretical study predicts the conductivity limited by charged-impurity scattering in STIs of the form²⁰

$$\sigma(n) \sim C \left| \frac{n}{n_{\text{imp}}} \right| [e^2/h] \quad \text{for } n > n^* \quad (1a)$$

$$\sigma(n) \sim C \left| \frac{n^*}{n_{\text{imp}}} \right| [e^2/h] \quad \text{for } n < n^* \quad (1b)$$

where $C = 169$ for Bi_2Se_3 on SiO_2 ²⁰ and n_{imp} is the charged impurity density. For $n^* < n < \sim 5 \times 10^{12}/\text{cm}^2$, we fit $\sigma(n)$ to Eqn. (1a) (figure 2a-dashed lines), to obtain $n_{\text{imp}} = 3.7, 5.5, 13$ and $8.9 \times 10^{13}/\text{cm}^2$ for device 1 run 1, device 1 run 2, device 2, and device 3, respectively. These high n_{imp} values are of similar magnitude to the observed n -type carrier density before top-gating is initiated in Device 1 run 1 ($\sim 3.1 \times 10^{13} \text{ cm}^{-2}$), indicating that the dopants act as charged impurities (see Supplementary Information). The increase in n_{imp} with further electrolytic gating (run 2) indicates electrochemical damage, likely solvation of Se ions. The observation of sublinear $\sigma(n)$ at $n < n_{\text{bulk}}$ in Device 3 may indicate that there are additional types of disorder, e.g. neutral point defects, which need to be considered.

The observed minimum conductivity of graphene can be well understood through Eqn. (1b) as due to the residual carrier density n^* in electron and hole puddles induced by the charged impurity potential at nominally zero carrier density: $\sigma_{\text{min}} = n^* e \mu$, where n^* is calculated self-consistently¹⁹. We adapt the self-consistent theory¹⁹ to the Bi_2Se_3 surface state, with degeneracy of one and effective dielectric constant $\kappa = 50$ (average of dielectric constants of Bi_2Se_3 and surrounding media). The adjustable parameter is d the distance of the charged impurities to the 2d electron system (graphene, or Bi_2Se_3 surface). Figure 3 shows the experimentally observed residual density n^* per surface for each device as well as σ_{min} per surface. We see qualitative

agreement between experiment and theory in that (1) σ_{\min} is non-universal and weakly dependent on n_{imp} and (2) n^* increases with n_{imp} . Particularly for increasing disorder in the same device (Device 1 run 1 vs. run 2), n^* increases but σ_{\min} is nearly unchanged (arrows in Figs. 3a and 3b). Quantitative comparison of experiment and theory yields an unphysically small $d = 1 \text{ fm} - 0.1 \text{ \AA}$, however the observed n^* and σ_{\min} are within a factor of 2 of the predicted values for reasonable $d \sim 1 \text{ \AA}$ corresponding to impurities located within the Bi_2Se_3 surface plane, such as Se vacancies. We consider this good agreement since the self-consistent approximation itself (equating the screening carrier density with the local Fermi energy) is not expected to be quantitatively exact.

We finally discuss the behavior of low field magnetotransport in the TI regime. Figure 4a shows the magnetoresistivity of device 1 (run 1) $\rho(H)$ per layer at various carrier densities. $\rho(H)$ curves at high $n > 5 \times 10^{12}/\text{cm}^2$ are nearly identical, but $\rho(H)$ changes significantly as the Fermi energy approaches the Dirac point¹⁵. In the limit of strong spin orbit interaction and low mobility, we can fit the low field magneto-conductance per surface to the simplified form of the theory for weak anti-localization²⁶,

$$\Delta\sigma(H) = A \frac{e^2}{h} \left[\ln \frac{H_0}{H} - \psi \left(\frac{1}{2} + \frac{H_0}{H} \right) \right] \quad (2)$$

where $H_0 = \hbar/4De\tau_0$ is a characteristic field related to the dephasing time τ_0 , ψ is the digamma function, and A is a fit parameter whose theoretically expected value is $1/2\pi$. Confining the fit to fields below 0.4 T, Eqn. (2) does provide reasonably good fits to the data at all carrier densities as shown in figure 4b. Fitting results across the carrier density range are shown in Figure 4c. At the charge neutrality point the coefficient A peaks at ~ 0.2 , which is within 25% of the theoretical value $A = 1/2\pi$ [15,16]. The observation of magnetoconductivity described by Eqn. (2) in the clear absence of bulk carriers confirms its surface state origin, as posited in Refs. 15 and 16. H_0

is maximum (indicating the coherence length is minimum) near $n = 0$; similar behavior is observed in the electron-hole puddle regime in graphene²⁷.

Electrolyte gating has allowed access to the transport properties of the Bi_2Se_3 surface in the topological insulator regime. We find that the electronic transport properties are consistent with the expected Dirac surface state in the presence of charged impurity disorder of density a few 10^{13} cm^{-2} limiting the mobility to 400 - 1000 cm^2/Vs . We identify the initial n -type dopants, defects induced by mechanical exfoliation, and damage due to electrolytic top gating as likely sources of the disorder. Reducing the disorder to the level seen in exfoliated graphene on SiO_2 ($n_{\text{imp}} \sim 2\text{-}5 \times 10^{11} \text{ cm}^{-2}$)²⁸ would increase the mobility two orders of magnitude to $\sim 10^5 \text{ cm}^2/\text{Vs}$, and mobilities exceeding $10^7 \text{ cm}^2/\text{Vs}$ are conceivable if the disorder can be reduced to the level seen in suspended graphene²⁹.

Methods

Bi_2Se_3 thin films were produced by micro-mechanical cleavage of bulk Bi_2Se_3 single crystals and deposited on doped Si covered with 300nm SiO_2 . Thin films with thickness about 10nm were identified using atomic force microscopy (AFM). Au/Cr electrodes were defined by electron-beam lithography (see inset of Fig. 1). It was found that brief (~ 10 seconds) selective surface treatment of the contact area with N_2 plasma before the deposition of metals enhanced ohmic conduction.

Top gating was achieved by using polymer electrolyte consisting of LiClO_4 and polyethylene oxide (PEO) in the weight ratio 0.12:1, as previously used for carbon nanotubes and graphene devices²³⁻²⁵. For dual gate operation, negative top gate voltage (-3V for device 1 and -7V for device 2) was applied at room temperature and the sample was subsequently cooled

down to temperature $T < 250\text{K}$. In order to enhance cooling power, small amount of N_2 exchange gas was flowed into the chamber. For all the low temperature measurements except for second run of device 1, the samples were cooled down to 250K in less than one minute after applying top gate voltage. Further tuning of carrier density was done by sweeping back gate voltage at cryogenic temperature.

Four-probe measurements of longitudinal and transverse electrical transport were conducted using Stanford Research Systems SR830 Lock in amplifiers and Oxford Instruments 15 T superconducting magnet. Hall voltage was recorded in both polarities of the magnetic field ($\pm 1\text{T}$) and anti-symmetrized to remove longitudinal voltage components. In transport experiments a small and reproducible hysteresis in $V_{g,0}$ ($\sim 2\text{V}$) was observed during forward and backward gate voltage scans. In consequence, resistivity and Hall data with same V_g scan directions were compared in this work. Best fits to Eqn. (1a) were determined using a least squares linear fit to $\sigma(n)$ in the linear regime, determined by identifying the region of roughly constant slope $d\sigma/dn$.

Thermal runs as described in the main text were performed for more than five different Bi_2Se_3 samples with qualitatively consistent results, however only for the four data sets shown here for three samples (and one data set for a more disordered sample capped with thin Al_2O_3 , see Supplementary Material) could the carrier density be tuned through the Dirac point.

Acknowledgements

The study of electronic transport in novel materials during electrochemical modification is supported as part of the Science of Precision Multifunctional Nanostructures for Electrical

Energy Storage, an Energy Frontier Research Center funded by the U.S. DOE, Office of Science, Office of Basic Energy Sciences under Award Number DESC0001160. Preparation of Bi_2Se_3 was supported by NSF MRSEC (DMR-0520471) and DARPA-MTO award (N66001-09-c-2067). NPB was partially supported by the Center for Nanophysics and Advanced Materials. The authors acknowledge useful conversations with S. Das Sarma, E. Hwang, D. Culcer and S. Adam.

Author Contributions

D. Kim conceived the electrolytic gating scheme. D. Kim and S. Cho fabricated devices, performed the electrical measurements with K. Kirshenbaum, and analyzed the data. N.P. Butch, P. Syers, and J. Paglione prepared single crystal Bi_2Se_3 starting material. D. Kim, S. Cho, and M.S. Fuhrer wrote the manuscript.

Additional Information

The authors declare no competing financial interests. Supplementary information accompanies this paper. Correspondence and requests for materials should be addressed to Michael S. Fuhrer (mfuhrer@umd.edu).

References

1. Fu, L., Kane, C. L. & Mele, E. J. Topological Insulators in Three Dimensions. *Phys Rev Lett* **98**, 106803 (2007).
2. Zhang, H. J. *et al.* Topological insulators in Bi_2Se_3 , Bi_2Te_3 and Sb_2Te_3 with a single Dirac cone on the surface. *Nat Phys* **5**, 438-442 (2009).
3. Hsieh, D. *et al.* A tunable topological insulator in the spin helical Dirac transport regime. *Nature* **460**, 1101-1105 (2009).
4. Chen, Y. L. *et al.* Experimental Realization of a Three-Dimensional Topological Insulator, Bi_2Te_3 . *Science* **325**, 178-181 (2009).
5. Xia, Y. *et al.* Observation of a large-gap topological-insulator class with a single Dirac cone on the

- surface. *Nat Phys* **5**, 398-402 (2009).
6. Zhang, T. *et al.* Experimental Demonstration of Topological Surface States Protected by Time-Reversal Symmetry. *Phys Rev Lett* **103**, 266803 (2009).
7. Alpichshev, Z. *et al.* STM Imaging of Electronic Waves on the Surface of Bi_2Te_3 : Topologically Protected Surface States and Hexagonal Warping Effects. *Phys Rev Lett* **104**, 016401 (2010).
8. Hanaguri, T. *et al.* Momentum-resolved Landau-level spectroscopy of Dirac surface state in Bi_2Se_3 *Phys Rev B* **82**, 081305R (2010)
9. Cheng, P. *et al.* Landau Quantization of Topological Surface States in Bi_2Se_3 *Phys. Rev. Lett.* **105**, 076801 (2010)
10. Steinberg, H., Gardner, D. R., Lee, Y. S. & Jarillo-Herrero, P. Surface State Transport and Ambipolar Electric Field Effect in Bi_2Se_3 Nanodevices. *Nano. Lett.* **10**, 5032-5036 (2010).
11. Qu, D., Hor, Y. S., Xiong, J., Cava, R. J., & Ong, N. P. Quantum Oscillations and Hall Anomaly of Surface States in the Topological Insulator Bi_2Te_3 *Science* **329** 821 (2010)
12. Xiu, F. *et al.* Manipulating Surface States in Topological Insulator Nanoribbons *Nat. nanotechnol.* **6**, 216 (2011)
13. Analytis, J. G. *et al.* Two-dimensional surface state in the quantum limit of a topological insulator. *Nat. Phys.* **6**, 960-964 (2010).
14. Peng, H. *et al.* Aharonov-Bohm interference in topological insulator nanoribbons. *Nat Mater* **9**, 225-229 (2010).
15. Chen, J. *et al.* Gate-Voltage Control of Chemical Potential and Weak Antilocalization in Bi_2Se_3 . *Phys. Rev. Lett.* **105**, 176602 (2010).
16. Checkelsky, J.G. Hor, Y.S., Cava R. J. & Ong N. P. Surface state conduction observed in voltage-tuned crystals of the topological insulator Bi_2Se_3 . *Phys. Rev. Lett.* **106**, 196801 (2010).
17. Novoselov, K. S. *et al.* Two-dimensional gas of massless Dirac fermions in graphene. *Nature* **438**, 197-200 (2005).
18. Hwang, E. H., Adam, S. & Das Sarma, S. Carrier Transport in Two-Dimensional Graphene Layers. *Phys. Rev. Lett.* **98**, 186806 (2007).
19. Adam, S., Hwang, E. H., Galitski, V. M. & Das Sarma, S. A self-consistent theory for graphene transport. *P. Natl. Acad. Sci. USA* **104**, 18392-18397 (2007).
20. Culcer, D., Hwang, E. H., Stanescu, T. D. & Das Sarma, S. Two-dimensional surface charge transport in topological insulators. *Phys. Rev. B* **82**, 155457 (2010).
21. Butch, N. P. *et al.* Strong surface scattering in ultrahigh-mobility Bi_2Se_3 topological insulator crystals. *Phys. Rev. B* **81**, 241301 (2010).
22. Kong, D. *et al.* Rapid Surface Oxidation as a Source of Surface Degradation Factor for Bi_2Se_3 . arXiv:1102.3935v1, (2011).
23. Das, A. *et al.* Monitoring dopants by Raman scattering in an electrochemically top-gated graphene transistor. *Nat. Nanotechnol.* **3**, 210-215 (2008).
24. Efetov, D. K. & Kim, P. Controlling Electron-Phonon Interactions in Graphene at Ultrahigh Carrier Densities. *Phys. Rev. Lett.* **105**, 256805 (2010).
25. Lu, C. G., Fu, Q., Huang, S. M. & Liu, J. Polymer electrolyte-gated nanotube field-effect carbon transistor. *Nano. Lett.* **4**, 623-627 (2004).
26. S. Hikami, A. I. L., Y. Nagaoka. Spin-Orbit Interaction and Magnetoresistance in the Two Dimensional Random System. *Prog. Theor. Phys.* **63**, 707 (1980).
27. Gorbachev, R. V., Tikhonenko, F. V., Mayorov, A. S., Horsell, D. W. & Savchenko, A. K. Weak localization in bilayer graphene. *Phys. Rev. Lett.* **98**, 176805 (2007).
28. Jang, C. *et al.* Tuning the effective fine structure constant in graphene: Opposing effects of dielectric screening on short- and long-range potential scattering. *Phys. Rev. Lett.* **101**, 146805 (2008).
29. Bolotin, K. I., Sikes, K. J., Hone, J., Stormer, H. L. & Kim, P. Temperature-dependent transport in suspended graphene. *Phys. Rev. Lett.* **101**, 096802 (2008).

Figure captions

Figure 1 Bi_2Se_3 thin film device. **a**, Schematic device structure and dual gate configuration.

The inset shows an optical micrograph of Device 1. **b**, Resistivity and **c**, sheet carrier density determined from Hall measurement as a function of back gate voltage for device 1 run 1 at various temperatures from 5 - 63 K indicated in caption. The dashed red line corresponds to a capacitance $C_{\text{g,tot}} = 28 \text{ nF/cm}^2$.

Figure 2 Transport properties of Bi_2Se_3 surface state. **a**, The conductivity per surface vs.

carrier density per surface $\sigma(n)$ at zero magnetic field for three different devices. The inset shows $\sigma(n)$ near the Dirac point. Measurement temperature is $T = 5 \text{ K}$ for device 1 (runs 1 and 2), 4.2 K for device 2, and 2 K for device 3. Dashed lines are fits to Eqn. (1a). Transport data for $n > n_{\text{bulk}} = 5 \times 10^{12}/\text{cm}^2$ are denoted as dotted curves. **b**, Hall carrier density per surface vs. carrier density measured at the same conditions as in (a). Dashed lines show residual density n^* (defined in the text) for device 1 run 1 and device 3 (black), device 1 run 2 and device 2 (red) **c**, Variation of field effect mobility as a function of carrier density. Dashed curves indicate the region $|n| < n^*$ within which electron and hole puddles dominate transport.

Figure 3 Minimum conductivity vs. charged impurity density. **a**, Residual carrier density n^*

vs. impurity density n_{imp} and **b**, minimum conductivity σ_{min} vs. n_{imp} . Lines indicate the result of the self-consistent theory of Ref.19 for different impurity- Bi_2Se_3 distances $d =$

10 fm (black), 0.5 pm (red), 0.1 Å (green), and 1 Å (blue). Open symbols are experimental data.

Figure 4 Magnetic field suppression of weak anti-localization. **a**, Low field magneto-resistivity curves of device 1 measured at different per surface carrier densities. **b**, Symmetrized conductivity change (symbols) vs. magnetic field at various per surface carrier densities. Solid curves are fit to Eqn. (2). **c**, Prefactor A (squares) and dephasing field H_0 (circles) obtained from fits to Eqn. (2).

Figure 1

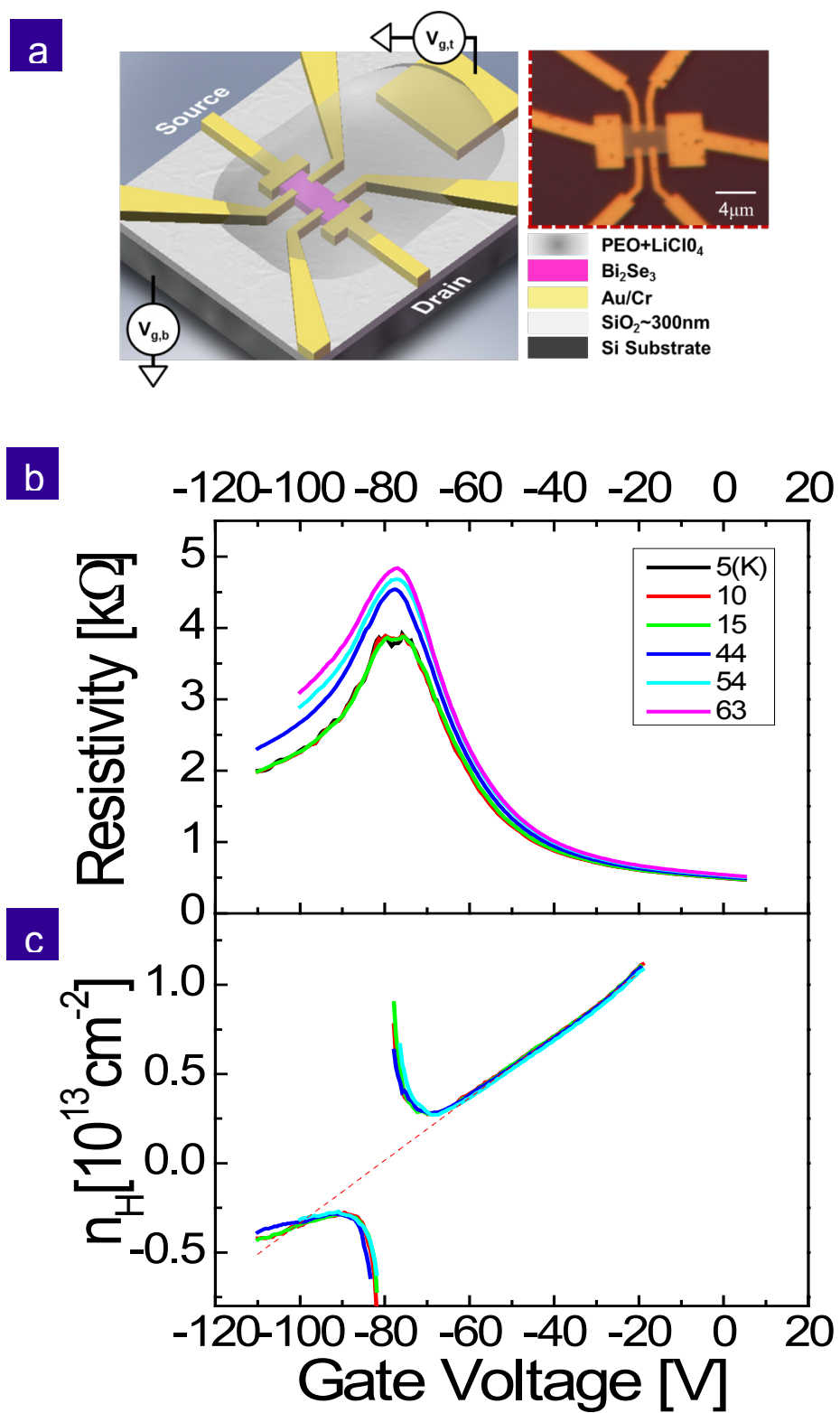


Figure 2

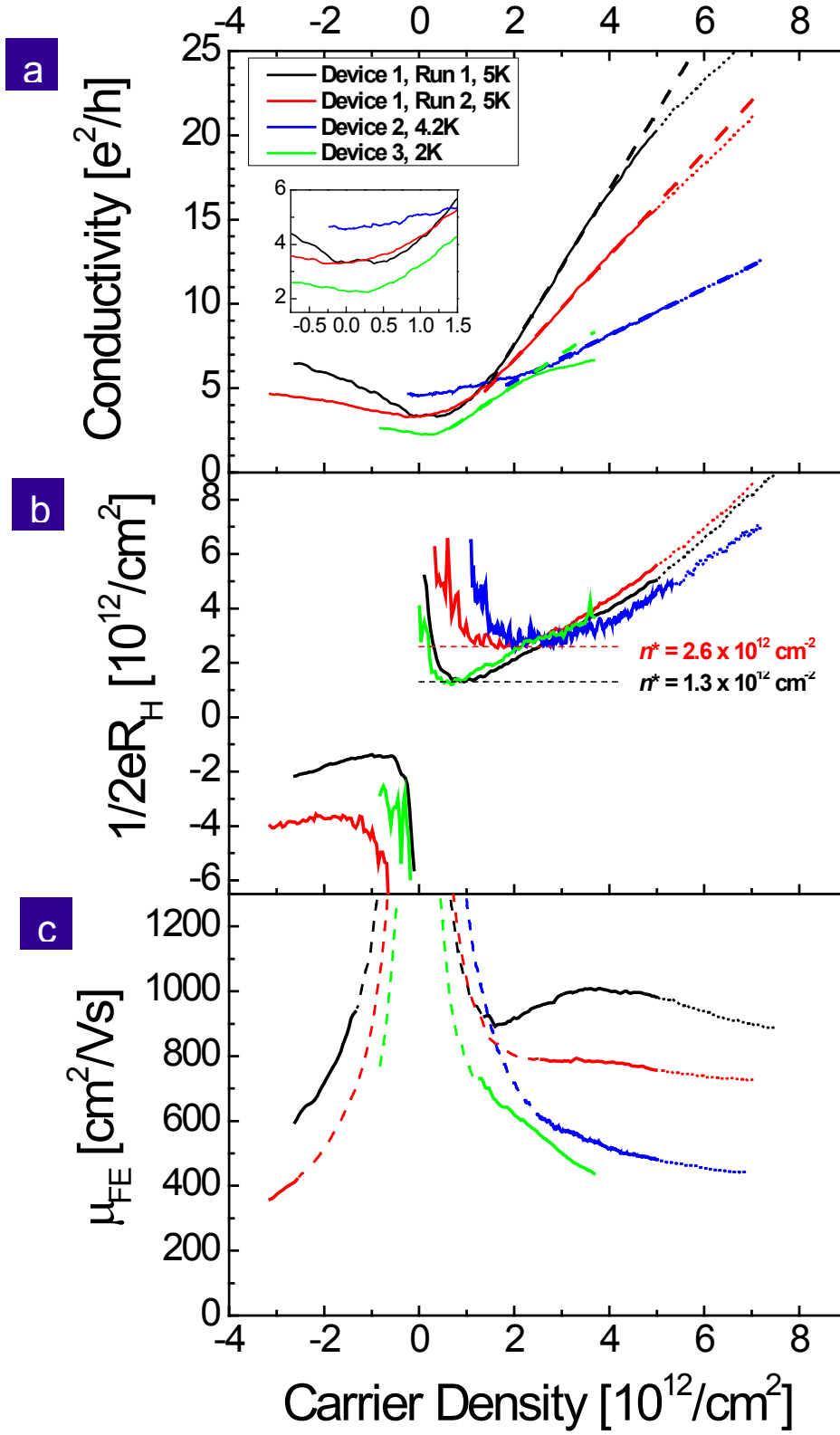


Figure 3

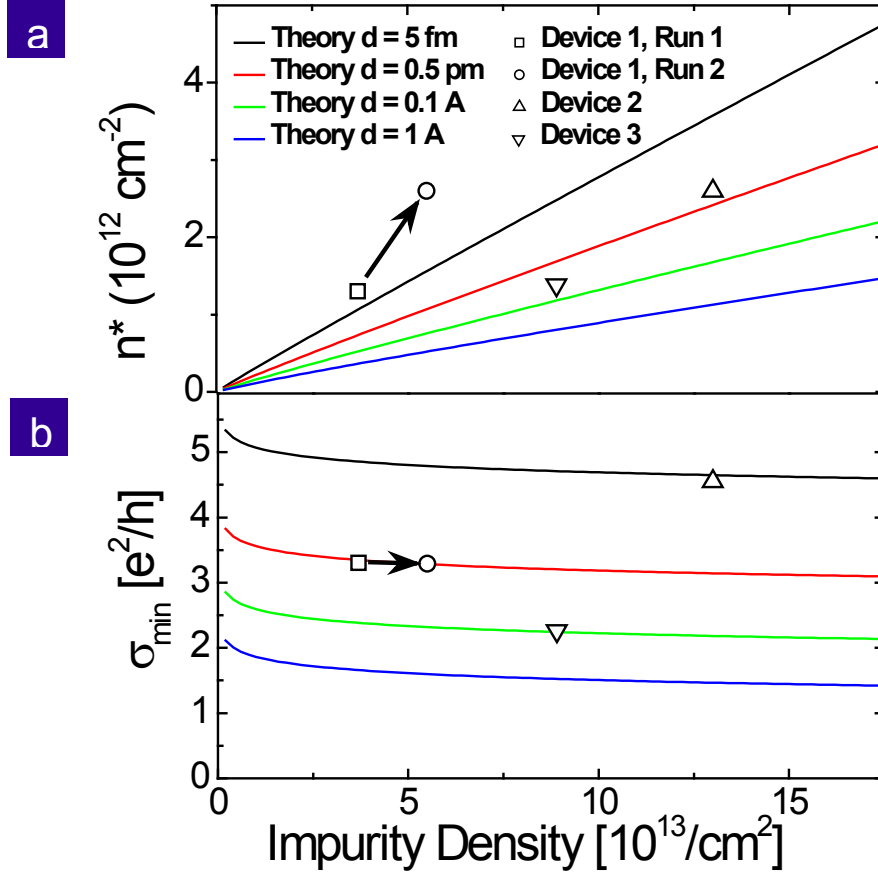
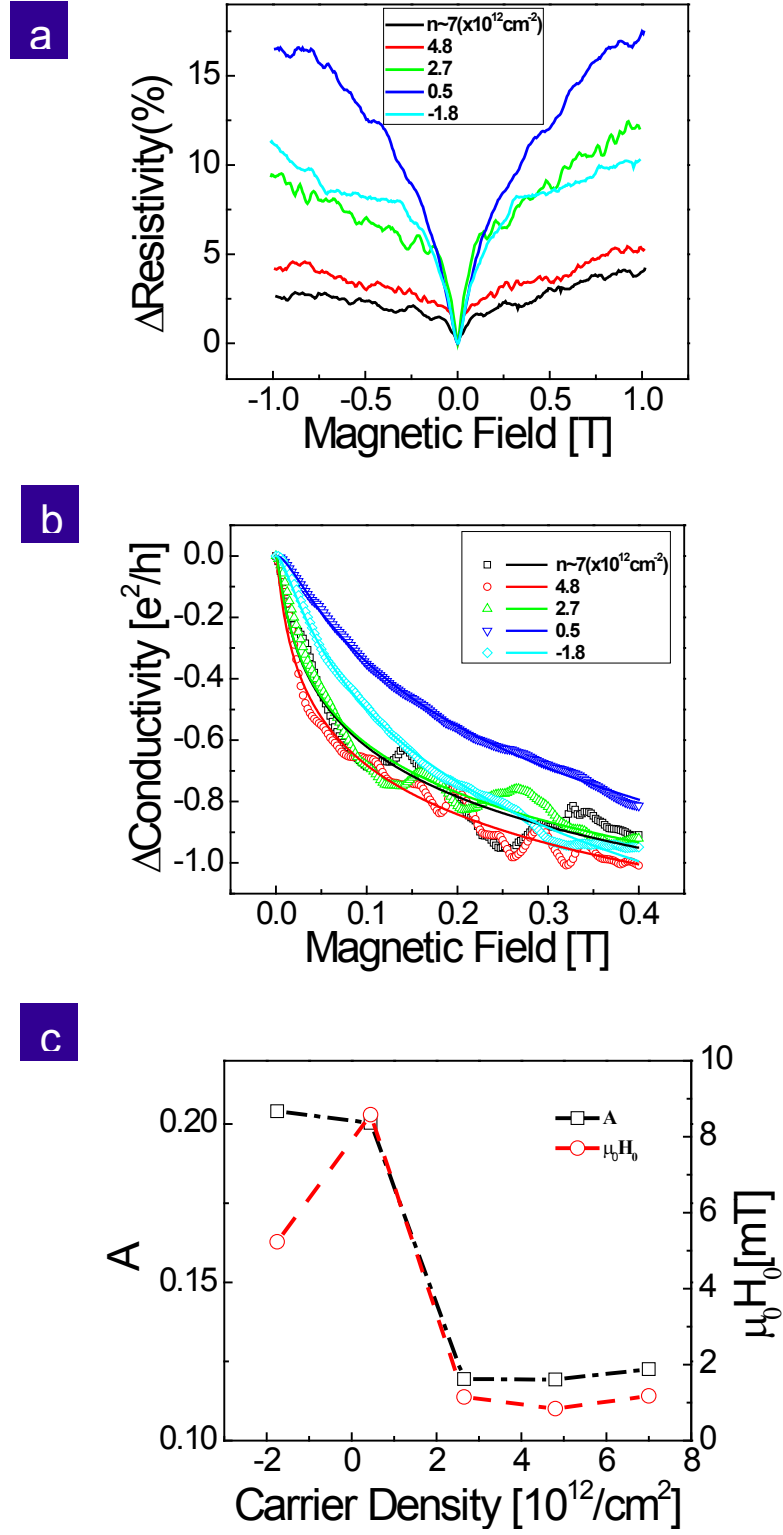


Figure 4



Minimum conductivity and charge inhomogeneity in Bi_2Se_3 in the topological regime

Dohun Kim*, Sungjae Cho*, Nicholas P. Butch, Paul Syers, Kevin Kirshenbaum, Johnpierre Paglione, and Michael S. Fuhrer[†]

Center for Nanophysics and Advanced Materials, Department of Physics, University of Maryland, College Park, MD 20742-4111, USA

Supplementary Information

1. Gate voltage induced carrier density per surface

We model the electrostatic response of the two topological surfaces to back gate voltage by the effective capacitor network as shown in figure S1a, which includes the electrostatic gate capacitances $C_{g,b}$ and $C_{g,t}$ to top and bottom surfaces respectively, and the quantum capacitances $C_{q,b}$ and $C_{q,t}$ of bottom and top surfaces. Note that the two surfaces are coupled by an interlayer capacitance C_{il} , which originates from the bulk part of the Bi_2Se_3 thin film. For the current devices, we estimate $C_{g,b} = 12 \text{ nF/cm}^2$, $C_{g,t} = 16 \text{ nF/cm}^2$, and $C_{il} \approx 9 \mu\text{F/cm}^2$. C_{il} is estimated from the thickness (10 nm) and bulk dielectric constant for Bi_2Se_3 ($\kappa \approx 100$)¹. The thickness is likely an overestimate since the surface electronic state has some finite extent into the bulk, thus C_{il} may be larger, reinforcing our results.

The quantum capacitance reflects the change in charge required to change the Fermi energy E_F in a material. For small changes in Fermi energy, C_q is often approximated by $e^2(dn/dE_F)$, where e is the elementary charge and dn/dE_F is the density of electronic states. Since

$D(E)$ varies significantly in a 2d Dirac material such as the topological surface state, we will use the full quantum capacitance $C_q = e^2(n/E_F)$ where n is the carrier density. We assume a linear dispersion relation for surface states in Bi_2Se_3 which is valid up to $n \approx 5 \times 10^{12}/\text{cm}^2$ per surface², thus considering degeneracy of one, $E_{\text{Fb}(t)} = 2\hbar v_F(\pi n_{\text{b}(t)})^{1/2}$ where \hbar is Planck's constant and $v_F = 6.4 \times 10^5$ m/s is the Fermi velocity in Bi_2Se_3 , representing roughly the average Fermi velocity for the conduction cone for energies below the bulk conduction band³⁻⁷. At the bulk conduction band edge of Bi_2Se_3 , $n_{\text{tot}} \approx 1 \times 10^{13}/\text{cm}^2$ and we use the experimentally observed $n_0 \approx 1 \times 10^{13}/\text{cm}^2$ at $V_g = -22\text{V}$ (see figure 1b in the main text) as a reference point; equal carrier density ($n_t = n_b = 5 \times 10^{12}/\text{cm}^2$) at this gate voltage was assumed. The carrier density of each surface can be expressed as

$$n_{b(t)} = n_{bg(tg)} \mp n_{il} \quad (1)$$

where $n_{bg(tg)} = C_{g,b(t)}(eV_g - E_{\text{Fb}(t)})/e^2$, $n_{il} = C_{il}(E_{\text{ft}} - E_{\text{fb}})/e^2$ and V_g is the applied back gate voltage.

Figure S1b shows calculated carrier density for bottom and top surface carrier densities as functions of back gate voltage. The results of the model above are shown in solid lines. For comparison, we also show carrier densities for the same parameters for gate capacitances in the weak coupling limit ($C_{il}/C_q \ll 1$, dotted lines). In this limit the ~30% difference in gate capacitances leads to the difference in gate voltage at charge neutrality ($\Delta V_{g,0}$) of ~20V, and carrier density difference Δn at $V_{g,0}$ of $\sim 2 \times 10^{12}/\text{cm}^2$, which is comparable to the observed region of combined electron and hole transport. However, the presence of large inter-surface capacitance enhances the tendency to equalize the surface charge densities. In our realistic coupling model (solid lines) $\Delta V_{g,0}$ is less than 4V and Δn is less than $0.3 \times 10^{12} \text{ cm}^{-2}$ (horizontal and vertical arrows in inset of figure S1b), supporting our argument that both surfaces are gated

to neutrality nearly simultaneously. Since Δn is much less than the observed n^* , we conclude that n^* is dominated by local inhomogeneity in the carrier density due to disorder. Therefore, as a good approximation, we can parameterize the transport properties as a function of carrier density per surface n estimated from $n_{\text{eff}} = (C_{\text{g,tot}}/2e)(V_{\text{g}} - V_{\text{g,0}})$ (blue dashed line) where $C_{\text{g,tot}}=28$ nF/cm².

2. Gate tuned transport of Bi₂Se₃ device 1 with polymer electrolyte at 300K

Figure S2 shows resistivity (ρ) and Hall carrier density (n_{H}) as a function of electrolyte gate voltage measured at 300K. Although the initial gate capacitance for the polymer electrolyte was found to be ~ 1 $\mu\text{F}/\text{cm}^2$, the gate efficiency decreased rapidly as the gate voltage exceeded -0.8V. Notable hysteresis in the forward and backward voltage scans was also found. However, we note that the possible mechanism which can cause hysteresis (e.g. polymer decomposition or reaction with the sample) is reversible in this voltage scan range (0-1V). Because of additional doping induced by mechanical cleavage and reaction with ambient species^{8,9}, the amount of total carrier density at zero gate voltage was found to be much greater than the expected considering the bulk charge density ($\sim 10^{17}$ cm⁻³) in our low-doped starting material¹. The observed initial doping level ($\sim 3.1 \times 10^{13}$ cm⁻²) is of similar magnitude to the n_{imp} obtained by fit to the theory of charged impurity governed conductivity in Bi₂Se₃² indicating that the dopants act as charged impurities.

3. Alumina(Al₂O₃) capped Bi₂Se₃ device

Motivated by recent reports^{8,9} showing surface degradation of Bi₂Se₃ upon exposure to atmosphere, we performed experiments of capping the surface with Al₂O₃. Thin (10nm) Bi₂Se₃ was mechanically exfoliated onto highly n-doped SiO₂ (300nm)/Si in a glove box of nitrogen

environment, transferred to an e-beam evaporator without exposing to ambient environment. Subsequently, very thin (1.5nm) alumina (Al_2O_3) was deposited at a base pressure of $\sim 10^{-7}$ Torr and the thin capping layer prevented Bi_2Se_3 surface from being exposed to air afterwards. Electrodes (Cr/Au) were prepared and electrical measurement with dual gate was done in the same way as described in the main text. Figure S3 shows conductivity and Hall carrier density measured at low temperature (4.2K). While we found it was possible to gate the sample through the Dirac point, we found Hall mobility of Al_2O_3 capped device $\sim 100 \text{ cm}^2/\text{Vs}$ (5~10 times lower than uncapped device of the same thickness), residual density $\sim 2 \times 10^{13} \text{ cm}^{-2}$ (4~8 times higher, and higher than the density at which bulk bands are populated). Following the analysis in the main text, we would extract a charged impurity density $\sim 2 \times 10^{14} \text{ cm}^{-2}$ (2-5 times higher), though the analysis is beyond its range of validity since the bulk bands are significantly populated. The result indicates that the capping layer itself may degrade the surface states by providing strong source of Coulomb charged impurities although capping surface may prevent further degradation of the surface from air exposure.

References

1. Butch, N. P. *et al.* Strong surface scattering in ultrahigh-mobility Bi_2Se_3 topological insulator crystals. *Phys Rev B* **81**, 241301 (2010).
2. Culcer, D., Hwang, E. H., Stanescu, T. D. & Das Sarma, S. Two-dimensional surface charge transport in topological insulators. *Phys Rev B* **82**, 155457 (2010).
3. Zhang, H. J. *et al.* Topological insulators in Bi_2Se_3 , Bi_2Te_3 and Sb_2Te_3 with a single Dirac cone on the surface. *Nat Phys* **5**, 438-442 (2009).
4. Hsieh, D. *et al.* A tunable topological insulator in the spin helical Dirac transport regime. *Nature* **460**, 1101-1105 (2009).
5. Xia, Y. *et al.* Observation of a large-gap topological-insulator class with a single Dirac cone on the surface. *Nat Phys* **5**, 398-402 (2009).
6. Hanaguri, T. *et al.* Momentum-resolved Landau-level spectroscopy of Dirac surface state in Bi_2Se_3 *Phys Rev B* **82**, 081305R (2010).
7. Cheng, P. *et al.* Landau Quantization of Topological Surface States in Bi_2Se_3 *Phys Rev Lett* **105**, 076801 (2010).
8. Kong, D. *et al.* Rapid Surface Oxidation as a Source of Surface Degradation Factor for Bi_2Se_3 . arXiv:1102.3935v1 (2011).
9. Analytis, J. G. *et al.* Two-dimensional surface state in the quantum limit of a topological insulator. *Nat Phys* **6**, 960-964 (2010).

Figure captions

Figure S1 Gate voltage induced surface charge density. **a**, Capacitor network model of Bi_2Se_3 thin film device. **b**, Calculated charge densities for top (black) and bottom (red) surfaces as a function of gate voltage. The inset shows $\Delta V_{g,0}$ and Δn (horizontal and vertical arrow, respectively, defined in text). The dotted lines are charge densities calculated in the weak interlayer coupling limit. Approximate carrier density per surface used in the main text is denoted by dashed blue line.

Figure S2 Electrolyte gating of device 1 at 300K. Resistivity (ρ) and sheet carrier density determined from Hall voltage (n_H) as a function of electrolyte gate voltage.

Figure S3 Electronic transport of Al_2O_3 capped Bi_2Se_3 device. Conductivity (σ) and Hall carrier density measured in an Al_2O_3 capped device at $T=4.2\text{K}$ as a function of back gate voltage.

Figure S1

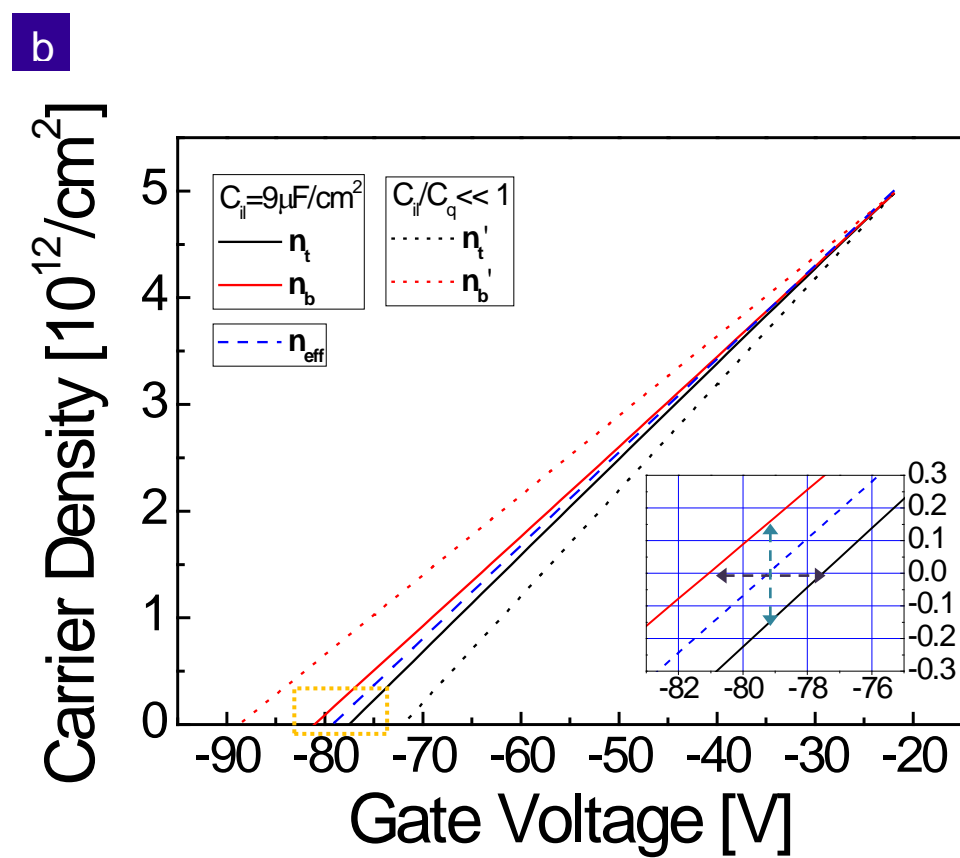
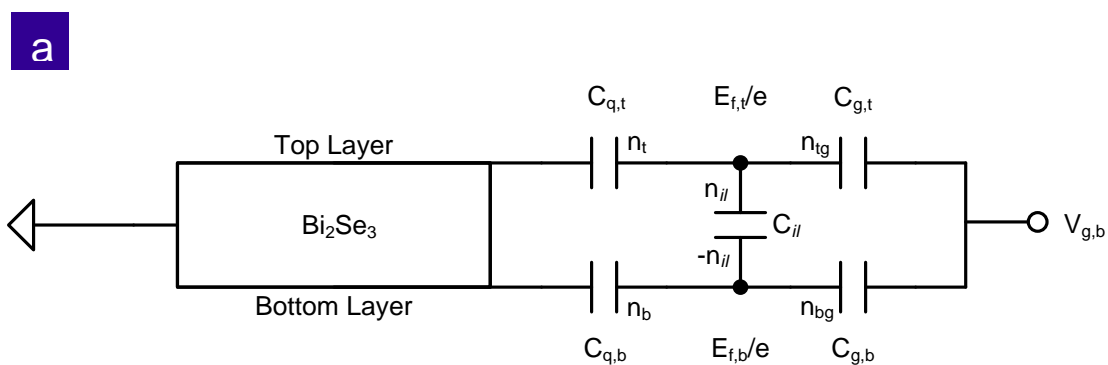


Figure S2

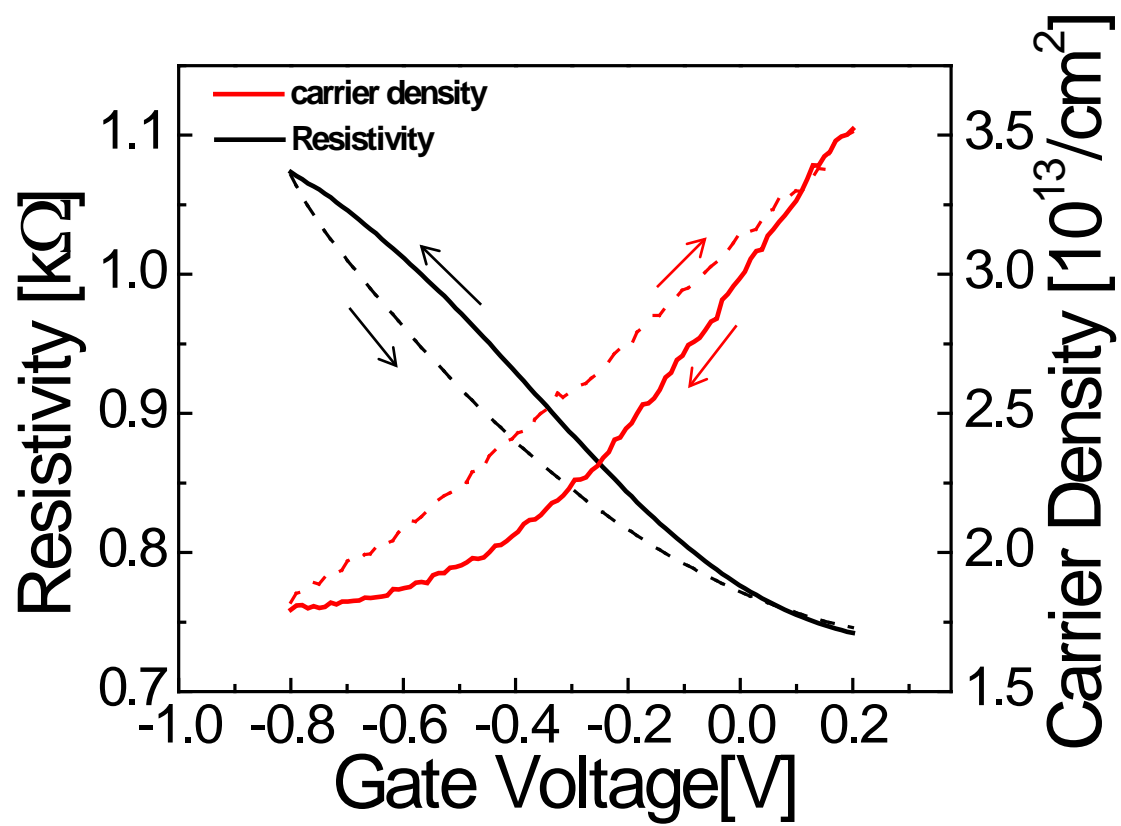


Figure S3

